Journal of Catalysis 262 (2009) 144–149

Contents lists available at ScienceDirect

Journal of Catalysis

www.elsevier.com/locate/jcat

Heterojunctioned $BiOCl/Bi_2O_3$, a new visible light photocatalyst

Seung Yong Chai [a], Yong Joo Kim [a], Myong Hak Jung [a], Ashok Kumar Chakraborty [a], Dongwoon Jung [b], Wan In Lee [a,*]

[a] Department of Chemistry, Inha University, Incheon, 402-751 Korea
[b] Division of Bio-Nano Chemistry, Wonkwang University, Iksan, Jeonbuk, 570-749 Korea

ARTICLE INFO

Article history:
Received 12 August 2008
Revised 14 December 2008
Accepted 19 December 2008
Available online 22 January 2009

Keywords:
Photocatalyst
$BiOCl/Bi_2O_3$
BiOCl
Bi_2O_3
Heterojunction
Visible light
Organic pollutant
CO_2

ABSTRACT

For the first time we report novel $BiOCl/Bi_2O_3$ photocatalyst functional under visible light irradiation. Even though both the individual BiOCl and Bi_2O_3 show very low photocatalytic efficiency under visible light irradiation, their heterojunctions provide unexpectedly high efficiency in decomposing organic compounds. Furthermore, the $BiOCl/Bi_2O_3$ can induce complete mineralization without formation of intermediate species by utilizing the holes generated in the VB of BiOCl. Compared to the Degussa P25, it demonstrates 5.7 times of efficiency in evolving CO_2 from gaseous 2-propanol (IP), and 10.5 times of efficiency in removing aqueous 1,4-terephthalic acid (TA) under visible light ($\lambda \geqslant 420$ nm) irradiation. In this $BiOCl/Bi_2O_3$ system the BiOCl seems to work as main photocatalyst, while the role of Bi_2O_3 is a sensitizer absorbing visible light. The photocatalytic mechanism has been proposed based on the relative band position of these two semiconductors.

1. Introduction

Removal of environmental pollutants through photocatalytic reaction has drawn increasing attention over the last few decades [1–3]. Among the various metal oxides and chalcogenides, TiO_2 has been known as the most efficient photocatalyst with its unique characteristics in band position, and surface structure. Due to its large band gap, however, TiO_2 can utilize only the photons in the wavelength shorter than 380 nm, which occupies no more than 4% of the solar spectrum. Therefore, the development of photocatalysts functional under visible light is indispensable in order to be able to utilize the major portion of the solar spectrum and to realize indoor application of photocatalyst.

Thus far, the major strategies for developing a visible light photocatalyst are modification of the TiO_2 band gap by doping [4–9], or development of new semiconductor materials capable of absorbing visible light. Recently, several new photocatalytic semiconductors including $BiVO_4$ [10,11], Bi_2WO_6 [12], $CaBi_2O_4$ [13], $PbBi_2Nb_2O_9$ [14], $Bi_4Ti_3O_{12}$ [15], and others [16–18], have been developed, but their photocatalytic efficiencies must be further improved in order to be suitable for practical applications. Another strategy to extend the light absorption property of TiO_2 is the formation of heterojunction between TiO_2 and narrow bandgap semiconductors [19–26]. So far, variety of coupled semiconductor systems, including CdS/TiO_2 [20], $CdSe/TiO_2$ [21], WO_3/WS_2 [22], CdS/AgI [23] and others, have been studied. Recently, several coupled systems such as $Bi_2O_3/SrTiO_3$ [24], Cu_2O/TiO_2, Bi_2O_3/TiO_2, $ZnMn_2O_4/TiO_2$ [25], TiO_2/Ti_2O_3 [26], etc. were reported to be efficient under visible light irradiation. However, the photocatalytic mechanism for the coupled system has not been systematically investigated, and no clear evidence was provided for the complete decomposition of organic pollutants under visible light.

In the heterojunction structure between TiO_2 and a sensitizer semiconductor with a narrow bandgap, the sensitizer is excited by visible light irradiation, and some of the photogenerated electrons or holes will then be transferred to TiO_2. Typically, metal chalcogenides such as CdS, and CdSe are used as sensitizer absorbing visible light [19–21,27]. Most of cases, the conduction band (CB) of the sensitizers is located higher than that of TiO_2. In this heterojunction system (denoted as A-type heterojunction) the electrons photogenerated by the sensitizer are transferred to the CB of TiO_2 with visible light irradiation, and these transferred electrons can initiate various reduction reactions. However, they lead to partial decomposition of pollutants in general, and it is difficult to evolve CO_2. On the contrary, if the VB level of sensitizer is lower than that of TiO_2 in the heterojunction structure (denoted as B-type heterojunction), some of the electrons in the VB of TiO_2 can be transferred to that of the sensitizer, and consequently the holes generated in the VB of TiO_2 can be used for oxidation reactions. Presumably, B-type heterojunction system can induce complete decomposition of pollutants, considering the powerful oxidative ability of the holes located in the VB of TiO_2. However, only a few

* Corresponding author. Fax: +82 32 867 5604.
E-mail address: wanin@inha.ac.kr (W.I. Lee).

0021-9517/$ – see front matter
doi:10.1016/j.jcat.2008.12.020

systems, utilizing the hole transfer between sensitizer and TiO_2, were reported so far [25,28], because it is difficult to find out appropriate sensitizers whose VB is lower than that of TiO_2.

In the present study, we report that the heterojunction structure between BiOCl and Bi_2O_3 can be an efficient photocatalyst under visible light irradiation, even though individual BiOCl and Bi_2O_3 show very low photocatalytic efficiency. BiOCl, with a bandgap of 3.6 eV, has been used mainly as a catalyst for the oxidative cracking of hydrocarbons [29], as photoluminescent material [30], and as pigment for cosmetics [31]. Recently, Zhang et al. reported that nanoparticular BiOCl can be an efficient photocatalyst in decomposing methyl orange in UV light [32]. This suggests that under UV light irradiation BiOCl is a potential photocatalyst which may compete with TiO_2, even though its band gap is considerably larger than that of the anatase TiO_2 ($E_g = 3.2$ eV). Bi_2O_3, with a band gap 2.6–2.8 eV, can absorb some portion of visible light ($\lambda < 440$ nm) [33–35], but alone, its photocatalytic activity is very low. For the first time it was found in this work that the heterojunction structure between BiOCl and Bi_2O_3 induces complete decomposition of gaseous 2-propanol to CO_2 under visible light irradiation, as well as it reveals much higher photocatalytic activity in decomposing organic compounds in gas or aqueous solution than the commercial TiO_2 (Degussa P25). Moreover, this new material is not harmful to environment, and the synthetic procedure is very simple with low production cost. Herein, we characterized the BiOCl/Bi_2O_3 heterojunction structures, and analyzed their photocatalytic properties. We also proposed a photocatalytic mechanism, based on the relative band position of these two semiconductors.

2. Experimental

One gram of bismuth(III) oxide powder (99.9%, Aldrich Chemical Co.) was dispersed in 10 mL of ethanol. Stoichiometric amount of the concentrated HCl was then added dropwise while the solution was vigorously stirred. The resultant suspension was stirred for 3 h and sonicated for 1 h at room temperature. After treatment with HCl, the yellowish color of Bi_2O_3 changed to white, which suggests that the surface of the Bi_2O_3 particle was converted to BiOCl, as illustrated in Scheme 1. The obtained white precipitates were washed several times with ethanol and heat-treated at 300 °C for 1 h. The relative ratio of BiOCl in BiOCl/Bi_2O_3 can be controlled by adjusting the amount of HCl added. Typically, a composite of 85 mol% BiOCl and 15 mol% Bi_2O_3 (denoted as 85/15 BiOCl/Bi_2O_3) was synthesized by adding 2.0 equivalents of HCl to Bi_2O_3, and 55/45 BiOCl/Bi_2O_3 was prepared by adding 1.8 equivalents of HCl.

X-ray diffraction (XRD) patterns were obtained for the BiOCl/Bi_2O_3 powder samples by using a Rigaku Multiflex diffractometer with monochromated high-intensity Cu$K\alpha$ radiation. The surface morphology of BiOCl/Bi_2O_3 powder samples was observed by a field emission scanning electron microscope (FE-SEM, Hitachi S-4200). Transmission electron microscope (TEM) images were obtained by a Philips CM30 operated at 250 kV. A methanol suspension of BiOCl/Bi_2O_3 particles was spread on a copper grid coated with holey amorphous carbon film. UV–vis diffuse reflectance spectra were acquired by a PerkinElmer Lambda 40 spectrophotometer. $BaSO_4$ was used as the reflectance standard. BET surface areas of the samples were measured with a surface area and porosimetry analyzer (UPA-150, Microtrac Inc.).

Photocatalytic activities of the prepared catalysts under visible light were evaluated by following two methods. First, 2-propanol (IP) in gas phase was used as a model compound. The several BiOCl/Bi_2O_3 and other photocatalytic samples were prepared as a form of particulate film. That is, the aqueous colloidal suspension containing 50 μmol of each photocatalytic sample was dropped and spread uniformly onto a 2.5×2.5 cm^2 Pyrex glass, and subsequently dried at 60 °C for 1 h. The whole area of the photocatalytic films was irradiated by a 300 W Xe lamp through a double-mounted UV cut-off filter (<420 nm, Oriel), and then through a water filter to remove UV and IR component. The power of visible light irradiated to the photocatalytic sample was 0.5 W/cm^2. The gas reactor system used for this photocatalytic reaction has been described elsewhere [36]. After evacuating the reactor, 0.08 μL of IP mixed in 1.6 μL of water was added to the 200 mL gas-tight reactor. Then the initial concentration of gaseous IP in the reactor was kept to 117 ppm in volume (ppmv). Thus the ultimate concentration of CO_2 evolved will be 351 ppmv when the whole IP is completely decomposed, as shown in the following equation.

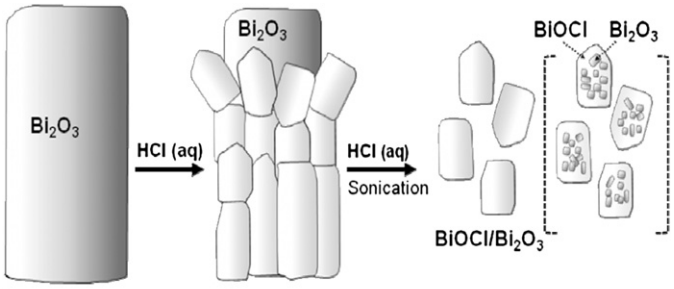

Scheme 1. Preparation principle of BiOCl/Bi_2O_3 heterojunction.

$$2(CH_3)_2CHOH(g) + 9O_2(g) \rightarrow 6CO_2(g) + 8H_2O(g).$$

The total pressure of the reactor was then controlled to 700 Torr by filling with oxygen gas. After a certain time of irradiation, 0.5 mL of the gas sample was automatically picked up from the reactor, and sent to a gas chromatograph (Agilent Technologies, Model 6890N). For the detection of CO_2, a methanizer was installed between the GC column outlet and the FID detector.

Second, for the photocatalytic degradation of 1,4-terephthalic acid (TA) in aqueous solution, 50 μmol BiOCl/Bi_2O_3 composites or other photocatalytic samples were suspended in 50 mL of 50 μM TA aqueous solution by magnetic stirring. The remnant TA after the irradiation of visible light was analyzed from its characteristic absorption peak detected by UV–vis spectrophotometer (Perkin–Elmer Lambda 40).

3. Results and discussion

The initial Bi_2O_3 purchased from Aldrich Chemical Co. was a rod-like structure with a diameter of 1–2 μm, as shown in Fig. 1a. By adding HCl, the surface of Bi_2O_3 was converted to BiOCl/Bi_2O_3, and its shape was gradually changed with increase of BiOCl content. In a low BiOCl composition, a granular BiOCl/Bi_2O_3 structure was formed on the surface of the Bi_2O_3 rods, as shown in the Fig. 1b. With increase of BiOCl compositions, the surface of the rod-like Bi_2O_3 structure was gradually collapsed to form primary nanoparticles, as shown in Fig. 1c (85/15 BiOCl/Bi_2O_3). By addition of excessive HCl, the well-defined pure BiOCl particles with a diameter of about 200 nm were formed (Fig. 1d).

The XRD patterns for BiOCl/Bi_2O_3 composites with molar ratios of 100/0, 85/15, 55/45, 40/60, and 0/100 are illustrated in Fig. 2. Pure Bi_2O_3 and BiOCl were the monoclinic α-phase [28] and tetragonal phase [26], respectively. With the increase of BiOCl component in BiOCl/Bi_2O_3 composites, the intensity of (120) peak at 27.42°, which is identified as the main peak of the remnant Bi_2O_3 phase, was gradually decreased, whereas that of the (101) peak at 25.86° inherent from the BiOCl phase was increased. No other phases were found in BiOCl/Bi_2O_3 composites, suggesting that there is no appreciable chemical reaction between BiOCl and Bi_2O_3. The BiOCl/Bi_2O_3 samples were annealed up to 450 °C in air,

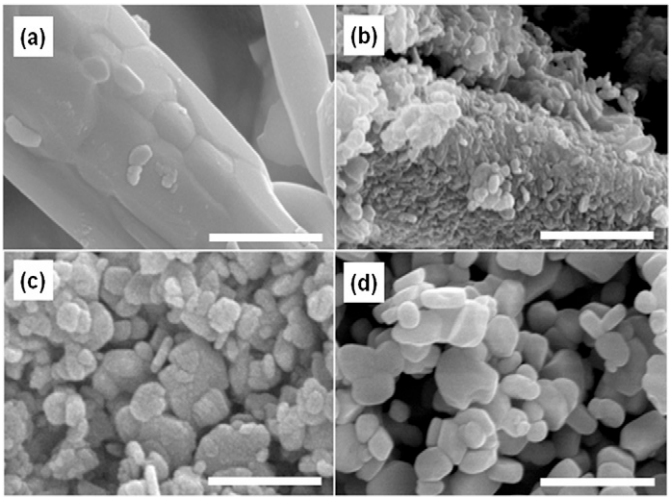

Fig. 1. SEM images of pure Bi_2O_3 (a), 40/60 BiOCl/Bi_2O_3 (b), 85/15 BiOCl/Bi_2O_3 (c), and pure BiOCl (d). Each scale bar is 1 μm.

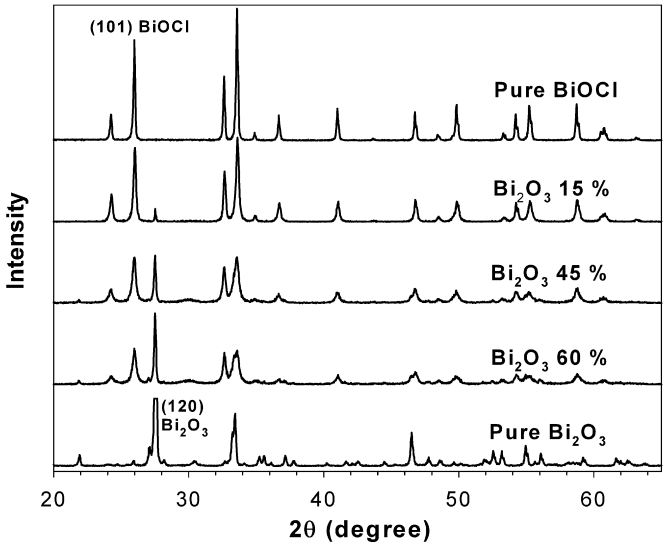

Fig. 2. X-ray diffraction patterns of Bi_2O_3, BiOCl, and several BiOCl/Bi_2O_3 in different compositions.

but the crystallinity of neither the BiOCl nor the Bi_2O_3 was noticeably changed.

Fig. 3 indicates the UV–vis diffuse reflectance spectra of BiOCl, Bi_2O_3, and BiOCl/Bi_2O_3 in several compositions. The bandgaps (E_g) of the BiOCl and Bi_2O_3, determined by extrapolation to the zero absorption coefficient, were 3.6 eV and 2.8 eV, respectively, corresponding to the results of the previous reports [32,34,35]. For BiOCl/Bi_2O_3 composites the absorbances in the 370–440 nm range decreased, as the component of Bi_2O_3 phase decreased. Therefore, those absorbance values could be used to estimate relative concentration of BiOCl and Bi_2O_3 in the composites by applying Beer-Lambert's law (the molar ratios of BiOCl to Bi_2O_3 indicated in this manuscript were estimated by this method).

For the characterization of the heterojunction structure between BiOCl and Bi_2O_3, the 85/15 BiOCl/Bi_2O_3 particles were embedded in a polymer matrix and sliced with 60 nm-thickness using an ultramicrotomy technique. The prepared specimens were then analyzed by TEM, as shown in Fig. 4. The TEM image in Fig. 4a reveals that the 85/15 BiOCl/Bi_2O_3 is a well-defined longish particle of ~200 nm width. It is difficult to obtain clear high-resolution TEM image for the Bi_2O_3 part, since Bi_2O_3 is much more vulnerable to electron beam irradiation than BiOCl. As shown in the high-resolution TEM image of Fig. 4b, the outer part of the BiOCl/Bi_2O_3 particle reveals a clear image, suggesting the presence of the crystallized BiOCl. The uniform fringe, with an interval of 0.73 nm, is in good agreement with the (001) lattice plane of the tetragonal BiOCl. On the other hand, as shown in Fig. 4c, the TEM image

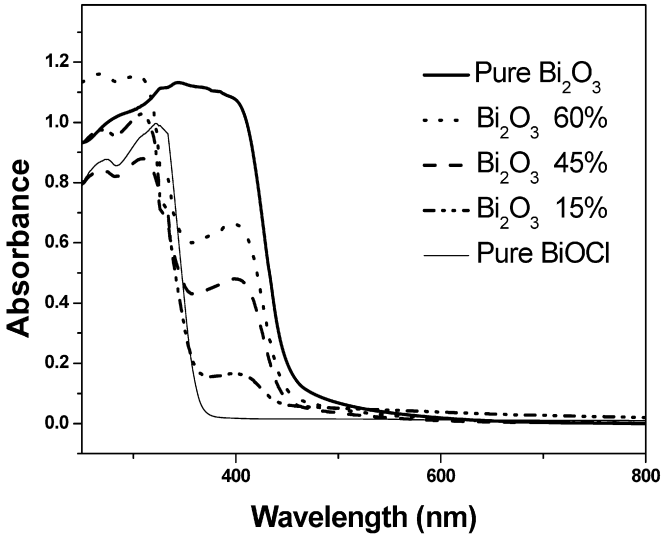

Fig. 3. Diffuse reflectance spectra of Bi_2O_3, BiOCl, and several BiOCl/Bi_2O_3 in different compositions.

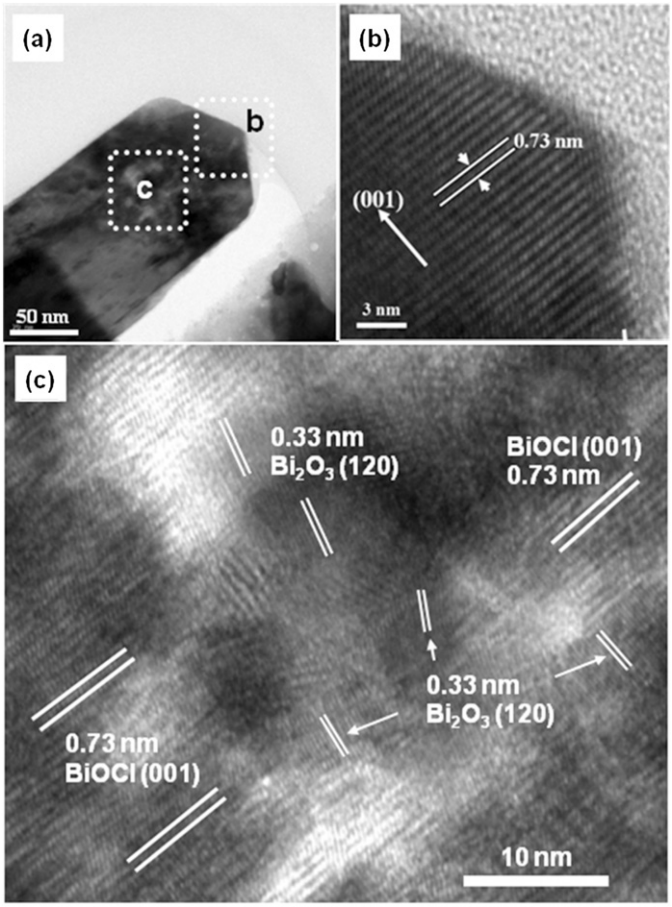

Fig. 4. TEM images for an 85/15 BiOCl/Bi_2O_3 particle. Typical TEM image (a), and HRTEM images for the outer (b) and inner (c) parts of the sample.

for the core of the $BiOCl/Bi_2O_3$ particle is not as clear as that of outer part, and several sets of mixed fringes are found, indicating the presence of the mixed phases of BiOCl and Bi_2O_3. That is, the interlayer distance of 0.73 nm corresponds to the (001) lattice plane of BiOCl, and that of 0.33 nm is consistent with the (120) plane of α-Bi_2O_3. These observations indicate that the nanosized Bi_2O_3 grains are embedded here and there inside the BiOCl matrix. For now compositional uniformity from particle to particle still remains in question, but it is clear that the BiOCl phase is positioned on the surface, while the some of the unreacted Bi_2O_3 remained inside in each $BiOCl/Bi_2O_3$ particle. Hence, the prepared $BiOCl/Bi_2O_3$ is considered to be a tightly-contacting heterojunction structure between BiOCl and Bi_2O_3 formed in nanosize level.

Photocatalytic activities of the $BiOCl/Bi_2O_3$ composites in decomposing organic compounds were evaluated under an irradiation of visible light ($\lambda \geqslant 420$ nm). First of all, gaseous IP was utilized as a model compound. It has been well known that IP first decomposes to acetone, and then finally mineralized to CO_2 [37]. The decomposition of gaseous IP approximated the first order kinetics. That is, the photocatalytic reaction is simply described by $-d[c]/dt = k[c]$, where $[c]$ is the concentration of IP, and k denotes the degradation rate constant. The removal of IP as a function of irradiation time is described in Fig. 5a. The $BiOCl/Bi_2O_3$ composites demonstrated notably high photocatalytic activities over a wide composition range, whereas the individual BiOCl and Bi_2O_3 showed a negligible efficiency. The calculated degradation rate constants (k_{IP}) in decomposing IP with several photocatalytic samples are shown in Table 1. Especially, the 85/15 $BiOCl/Bi_2O_3$ revealed the highest decomposition rate. That is, k_{IP} of the 85/15 $BiOCl/Bi_2O_3$ was 4.3 times that of Degussa P25. BET surface areas of the prepared photocatalysts are also given in Table 1. The surface areas of the $BiOCl/Bi_2O_3$ composites were much smaller than that of Degussa P25, and this seems to be caused by considerably larger particle size. For the comparison of conversion efficiency per unit catalytic surface area, a parameter of k_{IP}/A, where A is the surface area of the photocatalyst applied to the catalytic reaction, was determined, as shown in Table 1. The k_{IP}/A of the 85/15 $BiOCl/Bi_2O_3$ was 9.6 times as high as that of P25.

Fig. 5b describes the evolution of CO_2 as a function of irradiation time. The trend of CO_2 evolution, according to relative composition in the $BiOCl/Bi_2O_3$ composites, was very close to that of the IP removal. The highest photocatalytic activity was observed from the 85/15 $BiOCl/Bi_2O_3$ composite. That is, the evolved CO_2 after 2 h irradiation was 6.7 ppm, which was 5.7 times of that of P25.

Second, the photocatalytic activity of $BiOCl/Bi_2O_3$ was evaluated according to the removal of TA dissolved in aqueous solution. The remnant TA after the irradiation of visible light (>420 nm) was analyzed from its characteristic absorption peak by UV–vis spectroscopy. With approximating the photocatalytic degradation of TA as the 1st order kinetics, the plots of $\ln C$ vs. irradiation time for several catalytic samples were shown in Fig. 5c. The overall decomposition trend in aqueous solution was quite similar as that of the reaction in gas phase. The 85/15 $BiOCl/Bi_2O_3$ showed the highest photocatalytic activity. As shown in Fig. 5c and Table 1, k_{TA} (the degradation rate constant of TA) of the 85/15 $BiOCl/Bi_2O_3$ was 10.5 times that of P25 and 3.6 times that of $BiVO_4$, while k_{TA}/A of the 85/15 $BiOCl/Bi_2O_3$ was 26.4 times that of P25.

Both the BiOCl and the Bi_2O_3 showed very low photocatalytic activity under a visible light irradiation, but their heterojunctions demonstrated 10–50 times higher activity than the end-members. Presumably, the unusually high photocatalytic activity of $BiOCl/Bi_2O_3$ originates from the unique relative band position of these two semiconductors. The VB energy level of Bi_2O_3 [38] is expected to be considerably lower than that of BiOCl, since the VB of Bi_2O_3 originates from O2p, whereas that of BiOCl mainly comes

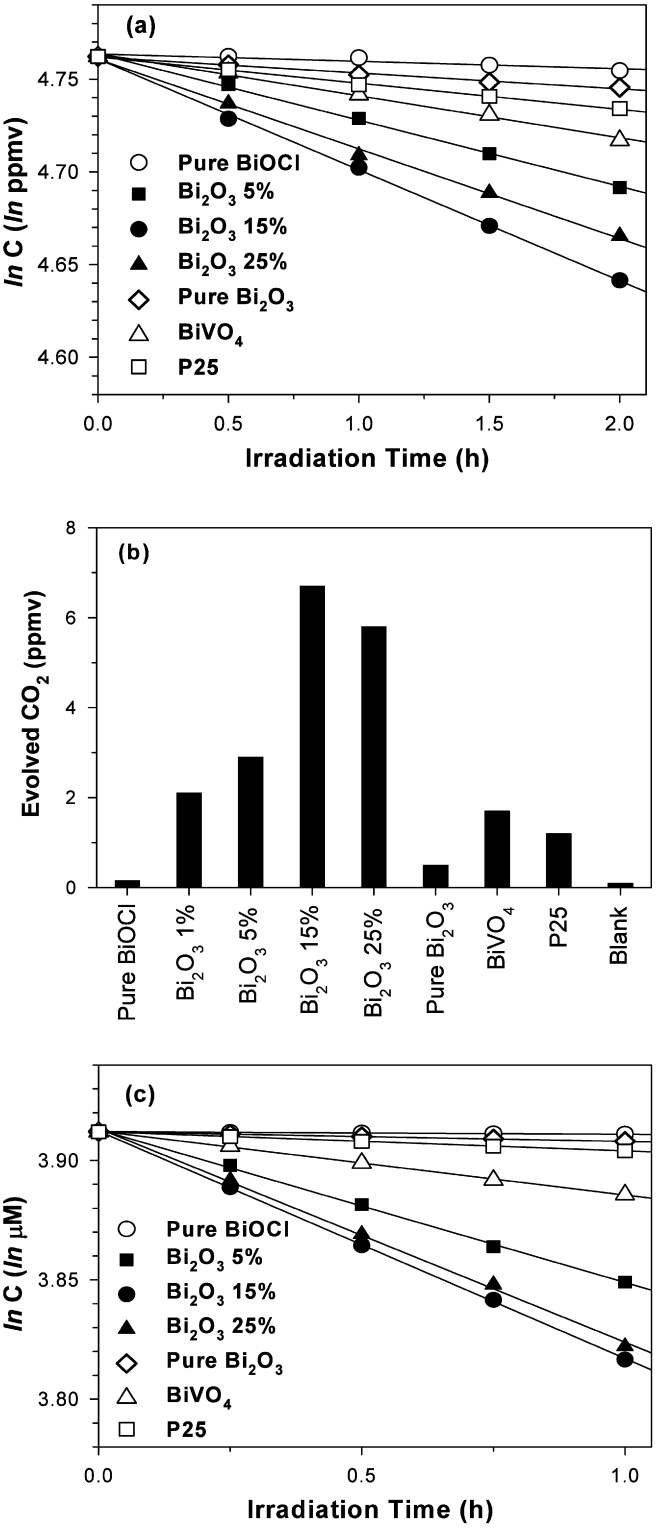

Fig. 5. (a) Photocatalytic removal of gaseous IP vs. irradiation time, and (b) CO_2 evolved in 2 hr under visible light irradiation (>420 nm). Initial concentration of the gaseous IP was 117 ppmv. (c) Photocatalytic removal of aqueous TA vs. irradiation time. The initial concentration of TA was 50 μM. The amount of each photocatalyst was 50 μmol in all photocatalytic experiments.

from Cl3p [32]. This was confirmed by our energy band calculation performed with the DFT method (see Supplementary Information). That is, the VB of Bi_2O_3 was lower than that of BiOCl by 0.7 eV, while the bandgaps of BiOCl and Bi_2O_3 were calculated to 3.55 eV and 2.75 eV, respectively.

Table 1
Surface areas and degradation rate constants of various visible-light photocatalysts in decomposing gaseous IP and aqueous TA.

Photocatalytic samples	BET surface area (m^2/g)	2-propanol (IP)		1,4-terephthalic acid (TA)	
		k_{IP} (h^{-1})	k_{IP}/A^a ($h^{-1}\,m^{-2}$)	k_{TA} (h^{-1})	k_{TA}/A^a ($h^{-1}\,m^{-2}$)
BiOCl	4.03	0.0034	0.075	0.0010	0.020
95/5 BiOCl/Bi_2O_3	5.14	0.0357	0.513	0.0640	0.919
85/15 BiOCl/Bi_2O_3	6.85	0.0603	0.602	0.0952	0.951
75/25 BiOCl/Bi_2O_3	7.29	0.0484	0.426	0.0895	0.788
Bi_2O_3	2.25	0.0085	0.163	0.0040	0.076
$BiVO_4$	7.21	0.0226	0.193	0.0267	0.228
Degussa P25	56.0	0.0141	0.063	0.0081	0.036

[a] *A* is the surface area of each catalyst (50 μmol) applied to the photocatalytic reactions.

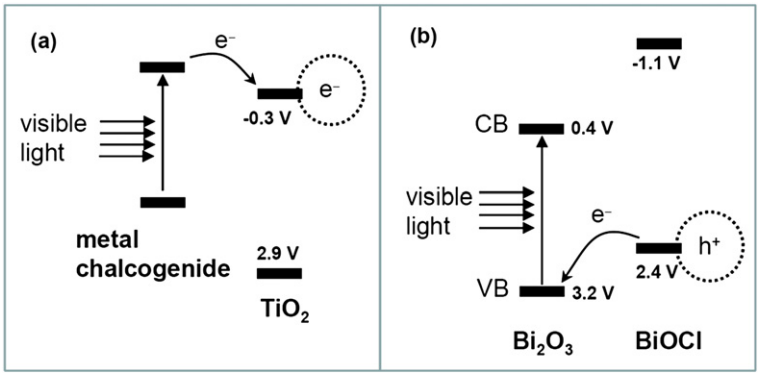

Fig. 6. Schematic diagram for energy band matching and flow of electrons for the TiO_2/chalcogenide systems (a) and BiOCl/Bi_2O_3 systems (b) during visible light irradiation.

Conventionally, metal chalcogenides with narrow bandgap have been loaded onto the surface of TiO_2 for the design of visible-light photocatalysts. By absorbing visible light the excited electrons in the metal chalcogenide are transferred to the CB of TiO_2, since its CB is generally positioned higher than that of TiO_2, as indicated in Fig. 6a. In this A-type heterojunction structure, the transferred electrons to the CB of TiO_2 can be used for photocatalytic reduction reactions. They can also be used for the decomposition of organic pollutant, but the complete mineralization to CO_2 is difficult, because the holes are not generated in the VB of TiO_2.

By contrast, the BiOCl/Bi_2O_3 heterojunction designed in this work is essentially different from A-type heterojunction structure. It has been reported that the BiOCl is a potential photocatalyst in decomposing organics under UV light irradiation [32]. Thus it is considered for the BiOCl/Bi_2O_3 that BiOCl works as a main photocatalyst, while the role of Bi_2O_3 is a sensitizer absorbing visible light. As indicated in Fig. 6b, the VB level of Bi_2O_3 is lower by 0.7 V than that of BiOCl. Hence this system is a kind of B-type heterojunction [22]. With irradiation of visible light, the electrons in the VB of Bi_2O_3 are excited to its CB. Thereby the VB of Bi_2O_3 is rendered partially vacant, and the electrons in the VB of BiOCl can be transferred to that of Bi_2O_3. As a result, holes are generated in the VB of BiOCl, and these initiate photocatalytic oxidation reactions. Therefore, with the irradiation of visible light, the BiOCl/Bi_2O_3 system can induce complete mineralization of organics. The observed CO_2 evolution, illustrated in Fig. 5b, is a clear indication for the complete decomposition of organics.

In the BiOCl/Bi_2O_3 prepared in this study, the BiOCl and Bi_2O_3 are tightly bound each other in nanosize level, since the Bi_2O_3 has been partially converted to BiOCl. Therefore, the hole-transfer through the junction will be greatly efficient. Moreover, the BiOCl working as main photocatalyst is located outer part of the BiOCl/Bi_2O_3 nanocomposite structure. Thus the effective catalytic sites are not screened by the formation of heterojunction structure. The BiOCl/Bi_2O_3 is safe for the environment, the synthetic procedure is simple, and it is easy to scale up with low manufacturing cost. More attention is necessary to this new heterojunction-type visible-light-photocatalyst.

4. Conclusion

The BiOCl/Bi_2O_3 system developed in this work is a new heterojunction-type photocatalyst working under visible light. The BiOCl/Bi_2O_3 demonstrates notably high photocatalytic activity over a wide composition range in decomposing IP in gas phase and TA in aqueous solution, whereas the individual BiOCl and Bi_2O_3 showed a negligible efficiency. Moreover, BiOCl/Bi_2O_3 induces complete decomposition of 2-propanol to CO_2. That is, the evolved CO_2 after 2 h irradiation was 6.7 ppm, which was 5.7 times that of Degussa P25 (12.8 times compared at unit catalytic surface area). It is considered for the BiOCl/Bi_2O_3 that BiOCl works as main photocatalyst, while the role of Bi_2O_3 is a sensitizer absorbing visible light. With irradiation of visible light, the electrons in the VB of Bi_2O_3 are excited to its CB. Thereby the VB of Bi_2O_3 is rendered partially vacant, and the electrons in the VB of BiOCl can be transferred to that of Bi_2O_3, since the VB level of Bi_2O_3 is lower by 0.7 V than that of BiOCl. As a result, holes are generated in the VB of BiOCl, and these initiate photocatalytic oxidation reactions. Therefore, with the irradiation of visible light the BiOCl/Bi_2O_3 system can induce complete mineralization of organics by utilizing the holes generated in the VB of BiOCl.

Acknowledgments

This work has been supported by the Ministry of Environment, Republic of Korea (Project No. 022-061-026).

Supplementary Information

Calculation results for the energy bands of BiOCl and Bi_2O_3 are provided in the Supplementary Information.

Please visit DOI: 10.1016/j.jcat.2008.12.020.

References

[1] C.S. Turchi, D.F. Ollis, J. Catal. 122 (1990) 178.
[2] M.R. Hoffmann, S.T. Martin, W. Choi, D.W. Bahnemann, Chem. Rev. 95 (1995) 69.
[3] A. Fujishima, T.N. Rao, D.A. Tryk, J. Photochem. Photobiol. C 1 (2000) 1.
[4] H. Yamashita, H. Harada, J. Misaka, M. Takeuchi, K. Ikeue, M. Anpo, J. Photochem. Photobiol. A 148 (2002) 257.
[5] H. Yamashita, M. Harada, J. Misaka, M. Takeuchi, B. Neppolian, M. Anpo, Catal. Today 84 (2003) 191.
[6] R.L. Putnam, N. Nakagawa, K.M. McGrath, N. Yao, I.A. Aksay, S.M. Gruner, A. Navrotsky, Chem. Mater. 9 (1997) 2690.
[7] X.T. Hong, Z.P. Wang, W.M. Cai, F. Lu, J. Zhang, Y.Z. Yang, N. Ma, Y.J. Liu, Chem. Mater. 17 (2005) 1548.
[8] R. Asahi, T. Morikawa, T. Ohwaki, K. Aoki, Y. Tao, Science 293 (2001) 269.
[9] S. Sakthivel, H. Kisch, Angew. Chem. Int. Ed. 42 (2003) 4908.
[10] A. Kudo, K. Omori, H. Kato, J. Am. Chem. Soc. 121 (1999) 11459.
[11] S. Kohtani, S. Makino, A. Kudo, Chem. Lett. 7 (2002) 660.
[12] J. Tang, Z. Zou, J. Ye, Catal. Lett. 92 (2004) 53.
[13] J. Tang, Z. Zou, J. Ye, Angew. Chem. Int. Ed. 43 (2004) 4463.
[14] H.G. Kim, D.W. Hwang, J.S. Lee, J. Am. Chem. Soc. 126 (2004) 8912.
[15] W.F. Yao, H. Wang, X.H. Xu, S.X. Shang, Y. Hou, Y. Zhang, M. Wang, Mater. Lett. 57 (2003) 1899.
[16] H. Irie, K. Hashimoto, J. Am. Ceram. Soc. 88 (2005) 3137.
[17] T. Murase, H. Irie, K. Hashimoto, J. Phys. Chem. B 108 (2004) 15803.
[18] J. Tang, J. Ye, Chem. Phys. Lett. 410 (2005) 104.
[19] N. Serpone, P. Maruthamuthu, P. Pichat, E. Pelizzetti, H. Hidaka, J. Photochem. Photobiol. A Chem. 85 (1995) 247.
[20] L. Spanhel, H. Weller, A. Henglein, J. Am. Chem. Soc. 109 (1987) 6632.
[21] D. Liu, P.V. Kamat, J. Electroanal. Chem. 347 (1993) 451.
[22] A.D. Paola, L. Palmisano, A.M. Venezia, V. Augugliaro, J. Phys. Chem. B 103 (1999) 8236.
[23] K.R. Gopidas, M. Bohorquez, P.V. Kamat, J. Phys. Chem. 94 (1990) 6435.
[24] H. Zhang, S. Ouyang, Z. Li, L. Liu, T. Yu, J. Ye, Z. Zou, J. Phys. Chem. Solids 67 (2006) 2501.
[25] Y. Bessekhouad, D. Robert, J.-V. Weber, Catal. Today 101 (2005) 315.
[26] H. Liu, W. Yang, Y. Ma, J. Yao, Appl. Catal. A Gen. 299 (2006) 218.
[27] J.C. Kim, J. Choi, Y.B. Lee, J.H. Hong, J.I. Lee, J.W. Yang, W.I. Lee, N.H. Hur, Chem. Commun. (2006) 5024.
[28] B. Gao, Y.J. Kim, A.K. Chakraborty, W.I. Lee, Appl. Catal. B Environ. 83 (2008) 202.
[29] N. Kijima, K. Matano, M. Saito, T. Oikawa, T. Konishi, H. Yasuda, T. Sato, Y. Yoshimura, Appl. Catal. A Gen. 206 (2001) 237.
[30] M.V. Shtilikha, D.V. Chepur, Sov. Phys. Semicond. 16 (1972) 962.
[31] G. Pfaff, P. Reynders, Chem. Rev. 99 (1999) 1963.
[32] K.-L. Zhang, C.-M. Liu, F.-Q. Huang, C. Zheng, W.-D. Wang, Appl. Catal. B Environ. 68 (2006) 125.
[33] P. Maruthamuthu, K. Gurunathan, E. Subramanian, M.V.C. Sastri, Int. J. Hydrogen Energy 19 (1994) 889.
[34] L. Zhang, W. Wang, J. Yang, Z. Chen, W. Zhang, L. Zhou, S. Liu, Appl. Catal. A Gen. 308 (2006) 105.
[35] A. Walsh, G.W. Watson, D.J. Payne, R.G. Edgell, J. Guo, P.-A. Glans, T. Learmonth, K.E. Smith, Phys. Rev. B 73 (2006) 235104.
[36] Y.T. Kwon, K.Y. Song, W.I. Lee, G.J. Choi, Y.R. Do, J. Catal. 191 (2000) 192.
[37] Y. Ohko, K. Hashimoto, A. Fujishima, J. Phys. Chem. A 101 (1997) 8057.
[38] Y. Xu, M.A.A. Schoonen, Am. Mineral. 85 (2000) 543.